Studies of Color Transparency Using Di-jet Events from a 190 GeV/c Pion Beam Scattered on Various Targets at COMPASS

Master's Thesis
by
Talayeh Aledavood

Physik-Department E18
Technische Universität München
May 2009

Contents

1 Introduction

Quantum Chromo Dynamics (QCD) is the theory which describes the interactions of quarks and gluons that interact strongly. Quarks and gluons are not observed as free particles but they are confined in hadrons. Interactions between these particles at short distances and for very short times can be described by perturbative QCD, while the non perturbative processes such as quarks confinement are still largely unknown. Color transparency is a phenomenon of perturbative QCD which is closely connected to the dynamics of confinement. The characteristic feature of this phenomenon is that small-size quark-gluon configurations interact with hadrons with small cross-sections.

One direct method to probe the color transparency phenomenon is to study diffractive dissociation of hadrons into di-jets. By using different target materials it is possible to compare the A-dependence of cross-sections with predictions of color transparency. The aim of this thesis is to study color transparency via this method.

The theoretical aspects of color transparency are explained in chapter 2. Different methods of studying color transparency are mentioned and diffractive dissociation of pions into di-jets is explained in more detail.

This thesis makes use of data recorded at COMPASS experiment during 2004 hadron beam time. There were various types of targets used in the experiment in addition to a $190\,\mathrm{GeV}/c$ π^- beam which make it feasible to study color transparency at COMPASS by studying the A-dependence of coherent diffractive cross-sections. An overview of the experiment and its physics programs can be found in chapter 3.
Properties of the data sample used for this analysis and different physical quantities associated to this data set are discussed in chapter 4.
One of the most important parts of this work was to normalize the luminosity. Two different methods were used for this purpose. These two methods and the results are presented in chapter 5.
Finding a suitable jet-finding algorithm and its realization and adoption for this analysis was a main challenge. This algorithm is discussed in detail in chapter 6.
Chapter 7 deals with experimental aspects of studying color transparency. Results of our analysis and the ones from previous experiments and theoretical predictions are presented in this chapter.
The last chapter summarizes this thesis and suggests different ways of improving the results. Besides, possibility of studying other physical quantities

using the same data sample and analysis methods is discussed.

2 Color Transparency

2.1 What is color transparency?

Color transparency (CT) is the name given to the prediction of perturbative QCD that small singlet systems of quarks and gluons interact with hadrons with small cross-sections[1]. This color neutrality may lead to suppression of initial and final state interactions of the small-sized systems or point like configurations (PLC), which are formed in hard processes. The requirement for observing CT effects is that PLC's are formed and that energies are sufficiently high that the non-expansion of the PLC is guarantied. This means that the PLC stays small enough while propagating through the nucleus and that it lives long enough to traverse distances longer than the size of the nucleus [Sea01, Fea93a, Hea06].
For observing CT, a selection of a sample of PLC's via hard exclusive reactions such as vector meson leptoproduction off nuclear targets, coherent photoproduction of J/ψ or diffractive di-jet production on nuclei, is required. We have the possibility to probe CT via the third process using COMPASS hadron beam data [Fea01]. In this method a high energy pion dissociates diffractively on a nuclear target imparting vary little energy to the target so that it does not break up. This is a coherent process in which the quark and antiquark in the pion break apart and hadronize into two jets. Unlike some of the other methods, studying diffractive dissociation of hadrons enables direct observation of color transparency in the A-dependence of diffractive di-jet production of pions.
The pion wave function can be expanded in terms of Fock states:

$$\Psi = \alpha|q\bar{q}\rangle + \beta|q\bar{q}g\rangle + \gamma|q\bar{q}gg\rangle + \cdots \tag{1}$$

At large momentum transfers (Q^2), the first (valence) component is dominant. According to counting rules, the other terms are suppressed by powers of $1/Q^2$ for each additional parton. If all the particles involved have relative velocities which are light-like, time dilation lengthens the lifetimes of these states and "freezes" the partonic content of the pion "seen" by other particles [Aea01].

There are two different pictures for the production of di-jets. Bertsch *et al.* [Bea83] proposed that the diffractive di-jets are materialization of the physically small $|q\bar{q}\rangle$ components of the pion wave function being filtered by the nucleus after the pion hits the nuclear target. In this quark gluon

[1] Brodsky and Mueller first introduced the color transparency phenomenon to QCD in 1982.

picture, by definition, CT selects the first component of the hadron wave function while the other components are suppressed. Besides, each quark, connected to another one by hard gluon exchange carrying momentum of order Q, should be found within a distance of order $1/Q$. Therefore, at large Q^2, one selects a special configuration of the wave function where all connected quarks are close together, forming a small size color neutral configuration. The masses of such fluctuations are undefined.
In a more recent calculation, Frankfurt *et al.* proposed that production of high mass di-jets is due to coherent scattering of small fluctuations of the hadron from nuclei. Unlike in the quark-gluon picture, these small fluctuations (resonances) which are described in a hadronic basis, have fixed masses. By observing two final state jets which carry a total momentum very close to the incoming hadron momentum, one will be able to select the coherent superposition of these resonances or the $|q\overline{q}\rangle$ component of the hadron wave function (in the language of the first picture) [Aea01, Fea01, Hea06]. An illustrative diagram of this process is shown in Fig. 1.

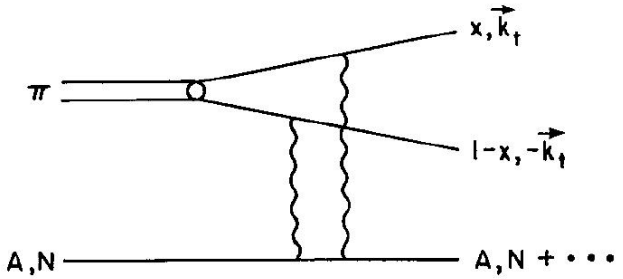

Figure 1: An illustrative diagram of dissociation of a pion into two jets. K_t denotes the transverse momentum [Fea93a].

2.1.1 Coherence length and cross-section probability function

In case a hadron with mass m and large momentum $p_{\rm lab}$, dissociates diffractively on a hadronic target T in the laboratory reference frame, the incoming hadron can fluctuate into a hadronic state with mass M^*. It follows from the uncertainty principle that the coherence length corresponding to the time, during which the incoming hadron stays in the state with mass M^* is given by [Fea02]:

$$l_c = \frac{1}{\Delta E} = ((\sqrt{M^{*2} + p_{\rm lab}^2} - (\sqrt{m^2 + p_{\rm lab}^2}))^{-1} \simeq \frac{2p_{\rm lab}}{M^{*2} - m^2} \qquad (2)$$

Equation 2 suggests that the coherence length grows with the energy of the incoming hadron (which is proportional to p_{lab}). At large enough energies, further fluctuations will be prohibited, so the hadron can be treated as frozen in its state.
If the coherence length is greater than the typical size of the target ($2R_T$),

$$l_c \geq 2R_T \tag{3}$$

then all the fluctuations, whose masses satisfy equations 2 and 3, interact coherently with the entire target.
The large l_c corresponds to small momentum transfers to the target. Therefore, the target (nucleon or nucleus) has a large probability to stay in its ground state in the course of the interaction. Besides, the coherence of the fluctuations means that they can be treated as frozen during the interaction with the target [Fea01]. This enables us to to treat the projectile as a coherent superposition of scattering eigenstates (each with an eigenvalue σ). $P(\sigma)$ is the probability to find a hadronic (quark-gluon) configuration, which interacts with the target with the cross-section σ, in the energetic projectile. This probability function can be reinterpreted by relating the size of a given configuration with its cross-section (e.g. in color transparency phenomenon a configuration with a small size has small interactions) [Fea93b].
It is possible to re-represent the incoming pion wave-function in this framework. $|\psi\rangle$ can be now represented as a coherent superposition of eigenstates $|\psi_k\rangle$ of the scattering matrix:

$$|\psi\rangle = \sum_k c_k |\psi_k\rangle \tag{4}$$

and

$$\sum_k |c_k|^2 = 1 \tag{5}$$

This formalism provides an economic way to take into account the composite structure of the incoming pion. Each state $|\psi_k\rangle$ scatters independently on the target (due to frozenness) with probability $|c_k|^2$. Therefore, the distribution over cross-sections $P(\sigma)$ can be written as:

$$P(\sigma) = \sum_k |c_k|^2 \delta(\sigma - \sigma_k) \tag{6}$$

It is required that $P(\sigma) \to 0$ at $\sigma \to \infty$.

2.1.2 Why is a pion beam convenient?

At low-σ, the quark counting rule fixes the behavior of $P(\sigma)$ for hadrons [Bea93]:

$$P_h(\sigma) \propto \sigma^{n_q-2} \tag{7}$$

where n_q is the number of valence quarks in the hadron. Since the number of valence quarks is different in protons and in pions, Eq. 7 predicts different behavior of cross-section probability functions of proton and pion projectiles. When σ is much smaller than the average value of the cross-section ($\sigma \ll \langle\sigma\rangle$), for protons it is expected that

$$P_p(\sigma) \sim \sigma \tag{8}$$

while it is predicted for pions that

$$P_\pi(\sigma) \sim \text{const} \tag{9}$$

The cross-section probability function for different hadrons can be estimated

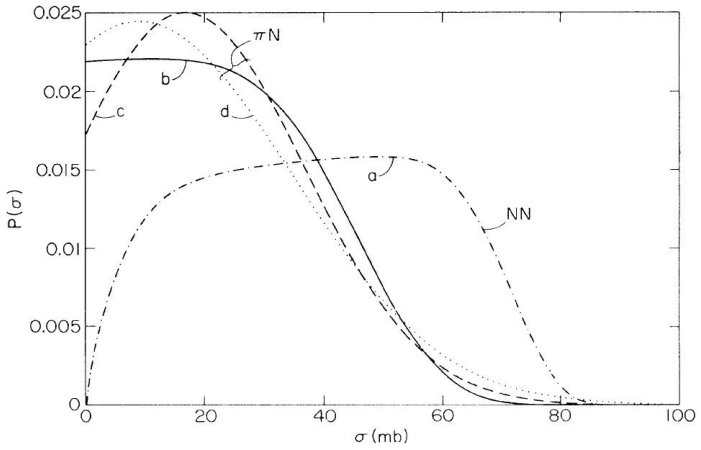

Figure 2: Cross-section probability functions for NN and πN scattering [Bea93].

by collecting information about the moments of the distribution. The first few moments of the distribution can be written as:

$$\int P(\sigma)d\sigma = 1 \tag{10}$$

$$\int P(\sigma)\sigma d\sigma = \langle\sigma\rangle \tag{11}$$

$$\int P(\sigma)\sigma^2 d\sigma = \langle\sigma^2\rangle = (1+w_\sigma)\langle\sigma\rangle^2 \tag{12}$$

The first equation is the normalization of $P(\sigma)$, and the first moment $\langle\sigma\rangle$ is the total hadron-nucleon cross-section. It can be shown that the quantity w_σ which appears in the third equation, is proportional to the amount of diffractive dissociation and therefore can be extracted from different experiments. More information on estimation of $P_p(\sigma)$ and $P_\pi(\sigma)$ based on their moments which are accessible via experimental data, can be found in [Bea93] and [Fea01]. Cross-section distribution functions for nucleon-nucleon scattering and pion-nucleon scattering are shown in Fig. 2. Three different sets of parameters (e.g. different w_σ's) are used in this plot, in order to estimate $P_\pi(\sigma)$. It can be seen, that for small cross-section, $P_\pi(\sigma)$ behaves very differently compared to $P_N(\sigma)$.
It is possible to estimate the probability for a pion to be in a point-like configuration, by calculating the integral $\int_0^{\sigma_{\max}} P_\pi(\sigma)d\sigma$ as a function of the upper limit $\sigma_{\max}$. This integral is plotted for both pion and nucleon in Fig. 3. It can be seen that pion has a much larger probability to be in a point-like configuration than the nucleon. More quantitatively, if we consider a configuration point-like if $\sigma < 5$ mb, the probability is about 10% for the pion and only $\approx 2\%$ for the nucleon [Bea93]. Therefore, pion is considered as a convenient projectile for studying color transparency via diffractive dissociation of hadrons into jets, which requires the hadron to be in a point-like configuration.

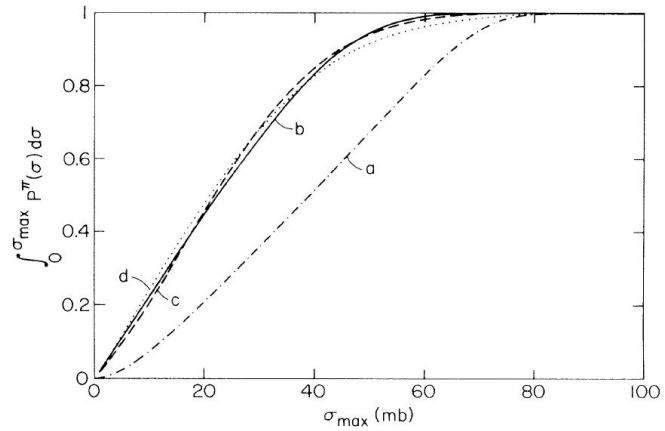

Figure 3: Probabilities of point-like configurations. Curves are the same as in Fig. 2 [Bea93].

2.2 Feasibility of investigating color transparency at COMPASS

In [Sea01] the potential of the COMPASS experiment for studying color transparency was studied by Sandacz *et al*. This study suggests that color transparency can be investigated in COMPASS via two separate processes:

- Exclusive vector meson production in hard muon-nucleus scattering and coherent production of jets with large relative transverse momenta: It is proposed to study color transparency via $\mu A \rightarrow \mu V A$ (coherent) and $\mu A \rightarrow \mu V N(A-1)$ (incoherent) exclusive vector meson production. Various target materials with different A can be used as well as a proton or deuteron target.

- Coherent production of jets with large relative transverse momenta which is studied in this thesis.

2.2.1 A similar study at Fermilab

The E791 experiment at Fermilab was a very high statistics experiment which was aimed at investigating the hadroproduction of charm quarks. The experiment was running from 1988 to 1992. The A-dependence of diffractive dissociation into di-jets of $500\,\mathrm{GeV}/c$ pions scattering coherently from carbon and platinum targets was studied in order to put light to the questions concerning the color transparency phenomenon [Aea01].

3 The COMPASS Experiment

COMPASS (Common Muon and Proton Apparatus for Structure and Spectroscopy) is a fixed-target experiment at the Super Proton Synchrotron (SPS) at CERN[2] [COM07]. The aim of the COMPASS experiment is to study in detail how nucleons and other hadrons are made up from quarks. Studying the hadron structure and hadron spectroscopy has been made possible by means of high intensity muon and hadron beams.
The COMPASS spectrometer was installed in 1999-2000 and was commissioned during a technical run in 2001. Data taking began in summer 2002 and continued until fall 2004. After a one year shutdown in 2005, COMPASS resumed data taking in 2006 [COMW]. The one year break gave the experiment a good chance for an upgrade. Since then, COMPASS has been taking data regularly. The 2009 beam time is scheduled to start in mid May.
Several research projects are underway in COMPASS which make use of different beams provided by the SPS beam line M2 that can deliver both muon and hadron beams. COMPASS employs different targets depending on the beam type and physical quantities to be measured. In 2004 for the first time, a pion beam was used for data taking. In this two-week pilot run, three different target materials were used: lead, carbon and copper. The aim of this running period was to study pion polarizability and diffractive dissociation of pions which is the subject of this thesis.
In this chapter the different physics programs at COMPASS are briefly explained. Besides, the COMPASS spectrometer is described as it was in 2004 and different types of beams, targets and various aspects of data taking and data analysis are explained.

3.1 Physics programs at COMPASS

The COMPASS experiment has been operating for nearly a decade. Huge amounts of data (up to 580 TB per year) of various nature have been stored during this time. This has given the COMPASS collaboration the chance to study many different physics topics. Some of these studies were planned before COMPASS started operating, but throughout the years of data taking, new ideas for measurements have been proposed. Some of the main fields of interest at COMPASS are explained in the following sections. These programs are categorized as muon programs and hadron programs in accordance with the beam type used in each program.

[2]European Organization for Nuclear Research, Geneva, Switzerland.

3.1.1 The muon program

Longitudinal spin structure of the nucleon: In the naïve quark model, it is assumed that the proton spin comes only from its valence quarks. Two up quarks and one down quark which contribute to a total spin projection of 1/2 of the proton. In the late 1980's the data from muon-proton scattering at CERN revealed that the spin or helicity contribution of quarks is surprisingly smaller than the predicted values of approximately 75% [Pre07] and that was when the proton spin crisis began. Since then many experiments have tried to reveal the source of the proton spin. COMPASS investigates the polarization of quarks $\Delta q(x)$ and gluons $\Delta G(x)$ inside nucleons by analyzing the deep inelastic muon scattering events. More specifically, the gluon contribution $(\Delta G/G)$ to the total nucleon spin is measured.

Transverse spin distribution functions: One of the functions which COMPASS is designed to fulfill is the investigation of the transverse polarized quark distribution functions $\Delta_T q(x)$ which have been known only since the 1990's to be needed for a full description of the quark state inside the nucleon. COMPASS measures the Collins and Sivers asymmetries of charged hadrons produced in deep inelastic scattering [Web04].

Lambda polarization: The spin-dependent quark distributions inside the nucleon and the fragmentation process of quarks can be studied via the production of Λ^0 hyperons in polarized deep inelastic. The Λ^0 hyperons act as natural polarimeters through their weak decay $\Lambda^0 \longrightarrow p\pi^-$ and are therefore a unique tool for studying polarization effects. At COMPASS, using a beam of longitudinally polarized muons with an energy of 160 GeV, Λ^0 polarization has been measured through its weak decay.

3.1.2 The hadron program

Pion polarizabilities: The deformation of mesons in the electromagnetic field of the γ during $\gamma\pi$ Compton scattering is characterized by the electric $(\overline{\alpha})$ and magnetic $(\overline{\beta})$ pion polarizabilities. These fundamental quantities depend on the rigidity of the pion's internal structure as a composite particle. The main goal of the COMPASS Primakoff physics program is to study the pion-photon interactions in order to investigate pion polarizabilities. In 2004, Primakoff events were recorded during the two week pilot run using pion scattering on a lead target [Moi03, Wei08].

Exotic mesons: One of the great ambitions of the COMPASS experiment is to detect exotic particles, i.e. strongly interacting particles other than mesons ($q\overline{q}$) and baryons (qqq). QCD puts no limit on the existence of exotic particles. In fact there are some hints towards their existence in theory. Availability of different types of beams at COMPASS (p, K, π and μ), provides an excellent opportunity for investigating these objects. COMPASS aims to confirm the existence of exotic particles by central production as well as diffractive scattering of different types of beam particles [Gra05].

3.2 COMPASS spectrometer

COMPASS is a two-stage spectrometer which can detect particles with a wide range of scattering angles and momenta. An artist view of the spectrometer is presented in Fig. 4. The large-angle spectrometer situated right after the target around the first dipole magnet SM1, investigates particles which have been scattered at large angles. The small-angle spectrometer SM2, detects particles of higher energy, scattered at smaller angles. In both stages detectors for track reconstruction and particle identification are deployed.SM1 which belongs to the large-angle stage has an integrated field strength of 1.0 Tm while SM2 which has to deal with particles with higher momenta has a higher integrated field strength of 4.4 Tm [Web04].

3.2.1 COMPASS setup during the 2004 pilot hadron run

Tracking detectors: There are many tracking detectors in COMPASS covering a wide range of time and position resolutions. These detectors which are spread all over the spectrometer are grouped into stations of the same type of detectors that are positioned very close to each other (approximately the same z-coordinate along the beam) but different detector planes in one station sit in different angles with respect to the beam line. The aim of these detectors is to reveal the trajectory of charged particles passing through them. By measuring the particle trajectory in different projections transverse to the beam direction, the track reconstruction will be done with less ambiguities.
Tracking detectors at COMPASS are categorized in three main groups: Very Small Area Trackers (VSAT), Small Area Trackers (SAT), Large Area Tracker (LAT).

- **Very small area trackers:** These trackers cover the beam region where the rate of beam particles is very high. Therefore, in this region detectors with excellent time or position resolution are required in order

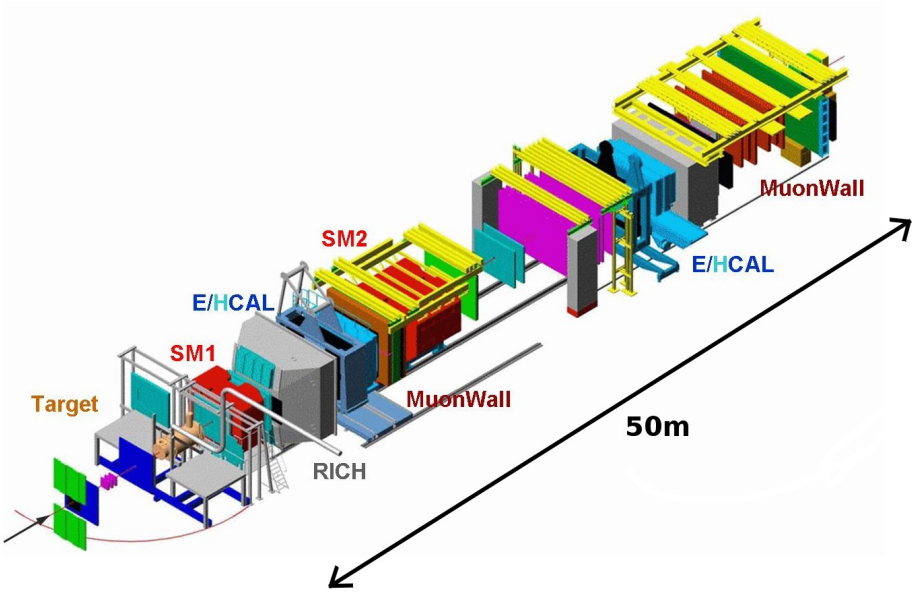

Figure 4: Artist view of the COMPASS experiment [Wei08]. The arrow on the left indicates the beam direction.

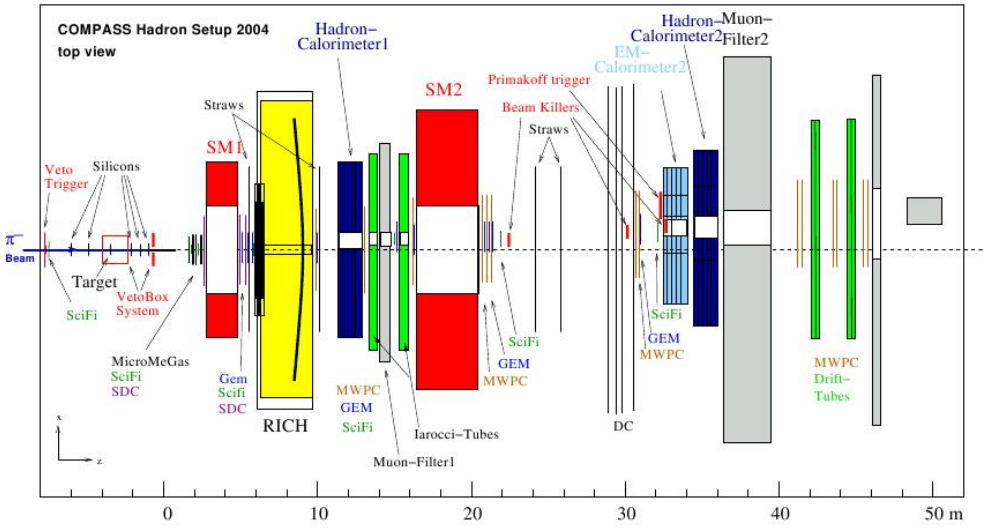

Figure 5: The setup of the COMPASS experiment during the 2004 pilot run [Wei08].

to identify hits belonging to the same track. This task is fulfilled by silicon microstrip detectors and scintillating fibres.
Silicon microstrip detectors which are used for the detection of incoming muon beam track, and, for the hadron program, for vertex and track reconstruction downstream of the target, have a spatial resolution of $8 - 11\,\mu$m and a time resolution of 2.5 ns [COM07].
Scintillating fiber detectors with a spatial resolution of $130\,\mu$m and a time resolution of 0.4 ns, provide tracking of incoming and scattered beam particles as well as all other charged reaction products in and very near the center of the primary beam [COM07].

- **Small area trackers:** The region at a radial distance of 2.5 cm to $15 - 20$ cm is called the intermediate region and is covered by the small area trackers. There are two different types of SAT's at COMPASS, which are both among novel detectors and are available only since few years ago. GEM[3] detectors and Micromegas[4] have been employed for the first time in a large-scale particle physics experiment.

- **Large area trackers:** These detector are used in the outermost regions. Drift chambers, straw tube chambers, multiwire proportional chambers and a large drift chamber are the detectors responsible for tracking in this region.

Particle identification: Several detectors in COMPASS fulfill the task of particle identification.

- **RICH:** The **R**ing **I**maging **CH**erenkov detector at COMPASS is used for hadron identification in the domain between $5\,\mathrm{GeV}/c$ and $43\,\mathrm{GeV}/c$. This detector which is located at the first spectrometer, separates hadrons to pions, kaons and protons [COM07]. This detector was filled with N_2 gas during the 2004 pilot run and therefore, was not used for particle identification.

- **CEDAR:** During the 2004 hadron program two CEDAR[5] detectors were installed but they did not function properly. These detectors were meant to tag pions and kaons in the beam. The working principle of these detectors is similar to that of the RICH detectors.

[3] **G**as **E**lectron **M**ultiplier
[4] Micro-Mesh Gaseous Structure
[5] **CE**renkov **D**ifferential counters with **A**chromatic **R**ings

- **Muon filters:** At the end of each spectrometer sits a muon filter which is made of a massive hadron absorber with tracking detectors at both sides. Muons are the only particles that can penetrate these massive walls and therefore can be detected by the tracking detectors right after the absorber.

Calorimetry: Two hadron calorimeters and one electromagnetic calorimeters were used in COMPASS in 2004 for energy measurements.

- **ECAL:** The electromagnetic calorimeter is a homogeneous calorimeter made of lead glass blocks. It is located before the second HCAL. It determines the energies of photons and electrons. The high energy gamma rays or electrons incident on the calorimeter produce electromagnetic showers inside the lead glass. Therefore, Cherenkov light is emitted by electrons and positrons in the shower on their way through the glass. The energy deposited in each counter is proportional to the amount of Cherenkov light which is emitted. The intensity of this light is measured by photo multipliers.

- **HCAL:** Both hadron calorimeters (HCAL1 and HCAL2) consist of layers of iron and scintillating plates. They are located just before the muon filter at the end of each stage. The HCALs are responsible for determination of hadron energies.

Trigger: The trigger system fulfills different tasks. It selects event candidates in a high rate environment and minimum dead time, to provide an event time reference and generate strobes for gating some of the analog-to-digital converters, and to trigger the readout of detectors and front-end electronics.

3.3 Beam properties

The beam line in the COMPASS experiment is provided by the SPS which has been operating at CERN since 1976 and provides the beam for many experiments at CERN such as the LHC. The M2 beam line which travels a 600 m path before it reaches the COMPASS hall, can be tuned for high-intensity muon beams up to 190 GeV/c in addition to high intensity hadron beam (mainly proton or mainly pion, positive or negative) beams up to 280 GeV/c. Negative muon beams are also available but with lower intensities. For testing and calibration purposes a tertiary electron beam can also be provided. This beam is used in COMPASS for absolute calibration of the

Beam parameters	Measured
Beam momentum	190 GeV /c
Hadron flux at COMPASS per SPS cycle	$\leq 10^8$
Proportion of negative pions	95%
Proportion of negative kaons	4.5%
Other components (mainly antiprotons)	0.5%
Typical spot size at COMPASS target ($\sigma_x \times \sigma_y$)	$3.5 \times 2.8\text{mm}^2$

Table 1: Beam parameters and performance of the 2004 hadron program [Wei08].

electromagnetic calorimeters. COMPASS production target T6 is a beryllium target with 500 mm thickness. The primary intense beam extracted from SPS impinges on the T6 target. If a low intensity beam is desired a thinner target can be used [Aea07]. The hadron beam properties (at the T6 target) are summarized in table 1.

3.4 Targets

Since COMPASS investigates various physical interactions, it requires different types of targets. Different types of targets, used in muon and hadron programs are explained in this section.

3.4.1 Targets of the muon program

The muon program at COMPASS requires a solid state polarized target which is much thicker than the targets common in experiments with electron beams. This is due to the limited flux of muons. The polarized target used in the COMPASS muon program which fulfills these requirements is deuterated Lithium (^{6}LiD). This target has been used in runs with the muon beam from 2001 until 2006. In 2007 the experiment started to use NH_3 as a polarized proton target (which can be polarized to a higher degree but has a lower fraction of polarizable matter) [Gra05, Lev08].

3.4.2 Targets of the hadron program

The COMPASS hadron program in 2004 used different solid state targets which were all simple disks with 3 cm diameters, corresponding to more than 3 sigma of the beam width. These targets had different thicknesses. In table 2 a list of the target materials and their characteristics can be seen.

Material	**Thickness (x)**	x/X_0	x/λ_I	**Atomic mass**
Lead	1.6mm	0.28	0.015	207.2
Lead	3 or 2 + 1mm	0.53	0.029	207.2
Copper	3.55mm	0.24	0.037	63.55
Carbon	23.5mm	0.12	0.086	12.01

Table 2: Targets of the 2004 hadron run [Wei08]. X_0 denotes the radiation length and λ_I the nuclear interaction length.

In 2004, data taking was mostly optimized for measuring pion polarizabilities via Primakoff scattering. In addition, the collected data was planned to be used for diffractive meson production studies.

3.5 Event reconstruction

The raw data from the experiment needs to be processed before it can be analyzed. For event reconstruction, COMPASS uses a fully object oriented program called CORAL[6] which is developed by the COMPASS collaboration (see Fig. 6). CORAL is also used to a lesser extent for analysis.
For the production process, not all the runs are used. The "good" runs have to be selected first. This is done in accordance with such criteria as detector performances, number of spills of the run, number of empty spills, etc. In the course of a run, such information is entered into a MySQL database. Passing this quality check, the chunks of the run are downloaded from tapes where they have been stored. CORAL reconstructs the tracks, particles and vertices in several steps.
The output of the reconstruction process is stored in a mDST[7] format. Between the input of raw data and the output mDST, the amount of the data is reduced by a factor of 100 [Aea07].

3.6 Data analysis

There are different softwares which contribute to different stages of data analysis at COMPASS. The main programs used for analysis are all developed internally at CERN (some even specifically for data analysis at COMPASS). These main tools of data analysis are explained in the following sections.

[6] **CO**MPASS **R**econstruction and **A**na**L**ysis
[7] **m**ini **D**ata **S**ummary **T**apes

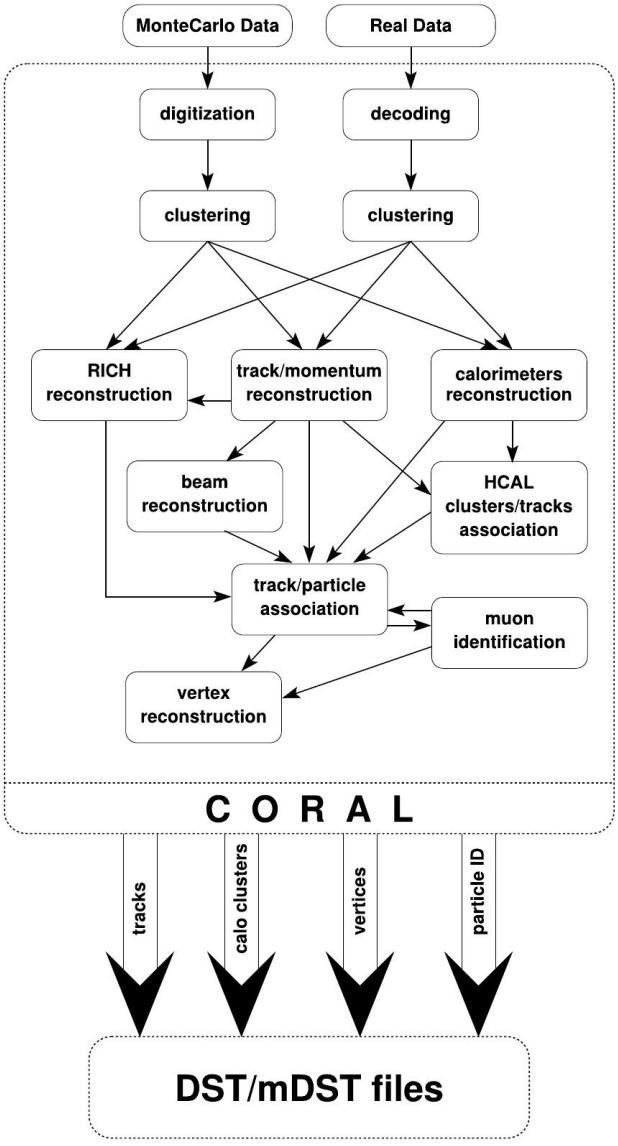

Figure 6: Schematic representation of the COMPASS reconstruction software.

3.6.1 ROOT

ROOT is an object-oriented data analysis framework, written in C++ and developed at CERN [ROO].
In ROOT, data can be stored in so called "trees". Each tree can have several branches depending on the number of quantities that are to be studied. Data can easily be accessed via the ROOT trees, cuts can be applied and physical quantities can easily be plotted and studied.

3.6.2 PHAST

PHAST[8] is a program which has been developed internally in COMPASS and is the main tool of all the experiment's physical analyses on the level of mDST. PHAST is an object oriented program written in C++ which provides dedicated classes and functions based on ROOT packages. It is also an environment for physics analysis code developments. To meet all the needs of an analysis it is possible to write ones own functions (which are called the UserEvent functions) and add them to the main code. The UserEvent functions are called every event. An event in PHAST contains an array of Vertices and an array of Particles. Events, Vertices and Particles in PHAST represent their physical equivalents. Events are passed to the UserEvent functions as arguments [PHAW].

[8] **PH**ysics **A**nalysis **S**oftware and **T**ools

4 Overview of the Analysis

In studying color transparency using the COMPASS 2004 hadron beam data, the same framework as the other analyses performed on COMPASS data is used. As explained in the previous chapter, PHAST provides the users with the possibility to tailor the data for each analysis individually. For this purpose, some UserEvent functions were written for this analysis. Primarily UserEvent functions are used to collect the right set of data out of the whole data set. While running PHAST for the analysis, these functions are called on every event and store all the information they have obtained in a ROOT tree.
Depending on the purpose of each step of analysis, some cuts are applied on the data set via these functions.

4.1 Data set

The analyzed data were recorded in three time periods during the two-week pilot hadron run in 2004. The start date and time, first and last run number, total number of analyzed runs, target materials and their thicknesses for all the three time periods are shown in Table 3. The beam type is π^- over all these runs.

In COMPASS all the runs are numbered consecutively. Since some runs

Target	**Cu**	**C**	**Pb**
Target Thickness	3.55 mm	23.5 mm	2 + 1 mm
From date	09-11-2004 21:38	10-11-2004 13:40	12-11-2004 17:09
To date	10-11-2004 13:19	11-11-2004 08:03	14-11-2004 22:10
From Run	43052	43086	43189
To Run	43085	43124	43323
Analyzed Runs	20	22	58
Analyzed Spills	2803	3545	8600

Table 3: Overview of the analyzed data

are only for testing or calibration purposes or have not passed the quality checks, only the runs which are designated “good runs” by the shift crew are taken into account for analysis.

4.2 Primary event selection

Before the process of analysis starts, a careful selection of the data set has to be performed. When dealing with an event via the UserEvent function, the first important aspect to investigate is whether this event contains a primary interaction or not. The products of primary interactions may undergo decays. Interactions of these decay products should not be confused with primary interactions of the beam particles. Thus, one of the event signatures is a primary vertex. If the vertex is a primary vertex (i.e. the vertex contains a beam particle as the incoming particle), other quantities of the event will be checked. If the event contains no primary vertex, it will be rejected.

4.2.1 Number and electric charge of the outgoing particles

The beam particles are pions with an electric charge equal to -1 e. Therefore, due to charge conservation the sum of electric charges of the outgoing particles should be equal to -1 e, too. When this analysis started and during the first few months, only events with 3 outgoing charged pions were taken into account. There was no reason to involve other final states in the analysis and besides the $\pi^-\pi^-\pi^+$ events had already been well studied at COMPASS and this could have been helpful for studying color transparency.
Later a method was introduced for this analysis which made use of any odd number of outgoing particles. This method will be discuses in the next chapter. All the plots shown in this chapter are based on the $\pi^-\pi^-\pi^+$ states.

4.2.2 Energy

One of the requirements of studying color transparency via diffractive dissociation of pions into jets is selecting exclusive events. In an exclusive event, the target stays intact and is neither excited nor destroyed in the course of the interaction and all secondary particles are reconstructed, that is the energy sum of all outgoing particles from the primary vertex (including the target recoil) matches the beam energy.
During 2004, the recoil particle was not detected and the beam energy was not measured. Therefore another procedure has to be applied in order to select exclusive events. Only the beam direction and hence the scattering angle were measured precisely by silicon detectors surrounding the target. The beam energy can be calculated based on the total energy of the outgoing particles and the scattering angle, assuming that the target particle remained intact throughout the scattering process [Cea08].
However, for selecting exclusive events a simplified method can be used. The energy of the beam particle (E_a) can be set equal to the sum of measured

energies of outgoing particles (E_c). This method was used for our analysis and the cut on energy was defined as $185 < E_c < 193\,\text{GeV}$ (see Fig. 7 and (Fig. 8).

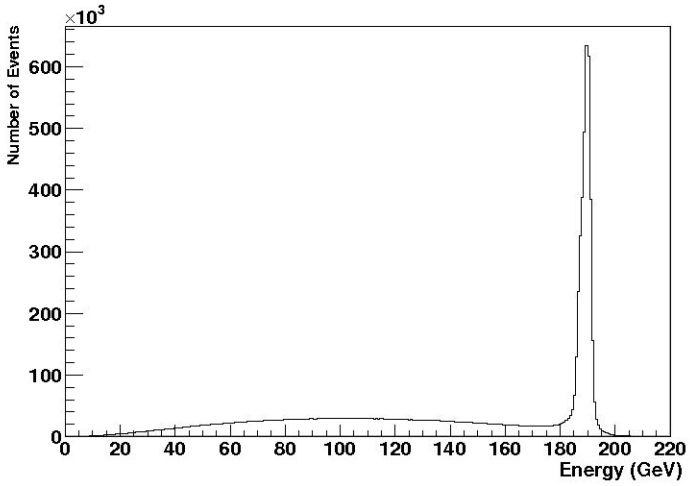

Figure 7: Energy distribution of outgoing particles ($\pi^-\pi^-\pi^+$), copper target.

4.2.3 Primary vertex position

The primary vertex position distribution along the beam axis is shown in Figure 9. A dominant sharp peak can be seen at about $z = -310\,\text{cm}$ which corresponds to the target.

Because this analysis is focused on A-dependence of the cross-sections it is very important that the events outside the target regions be discarded. The vertex position cut is tuned individually for each target because the thickness of the targets and their exact positions along the beam axis are different. This is done based on the width of the peak corresponding to the target in the primary vertex position distribution plot. A Gaussian function was fitted to these distributions . This fit is shown in Fig. 10 for the carbon target. 12σ of the Gaussian function to each side the mean value has been chosen as the target region. Even though, these fits are not very good but these target cuts work remarkably well for this analysis. Target cuts for different targets are shown in Figs 11, 12 and 13.

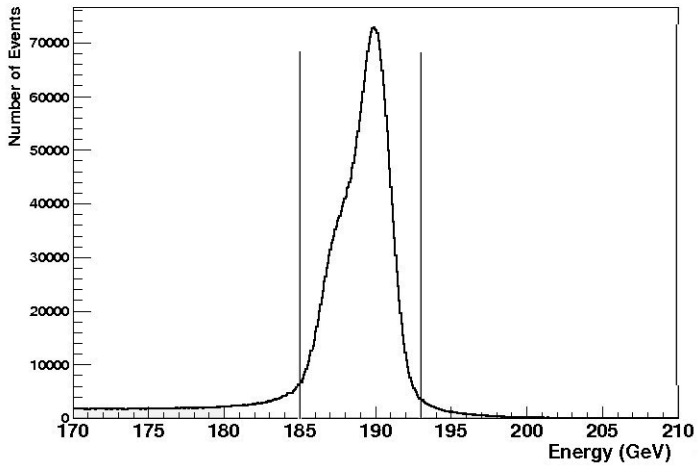

Figure 8: Energy distribution of outgoing particles ($\pi^-\pi^-\pi^+$), copper target. The exclusivity cut is shown by vertical lines.

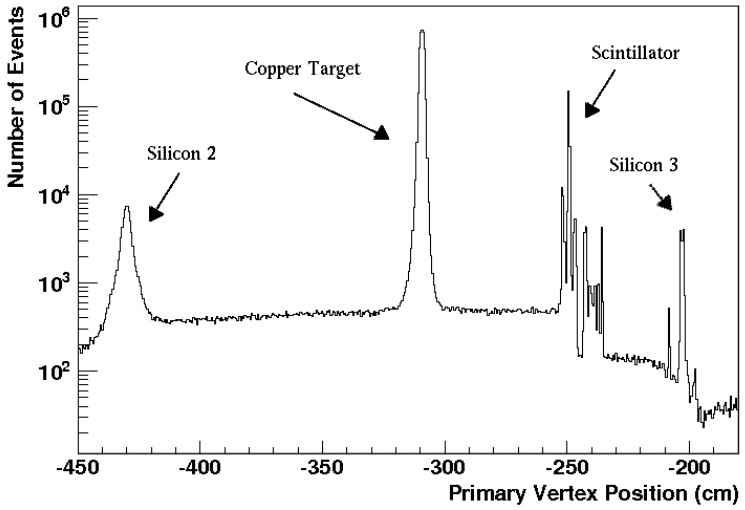

Figure 9: Vertex position along the beam axis

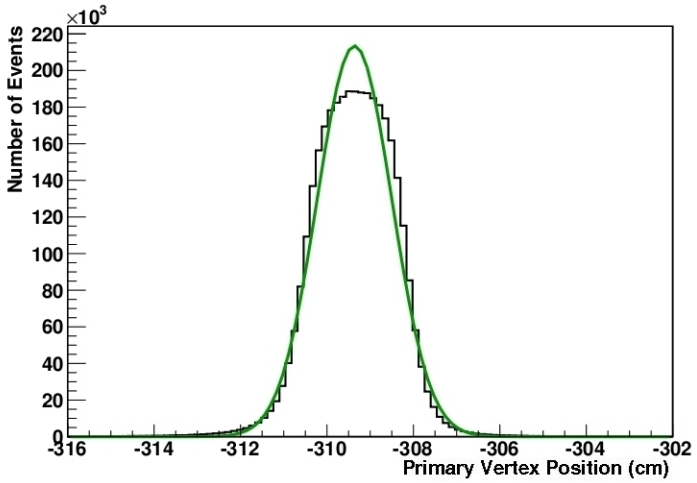

Figure 10: Primary vertex z position in the vicinity of the carbon target (logarithmic scale). The green curve represents a Gaussian fit to the distribution ($\sigma = 0.8670 \pm 0.0003$).

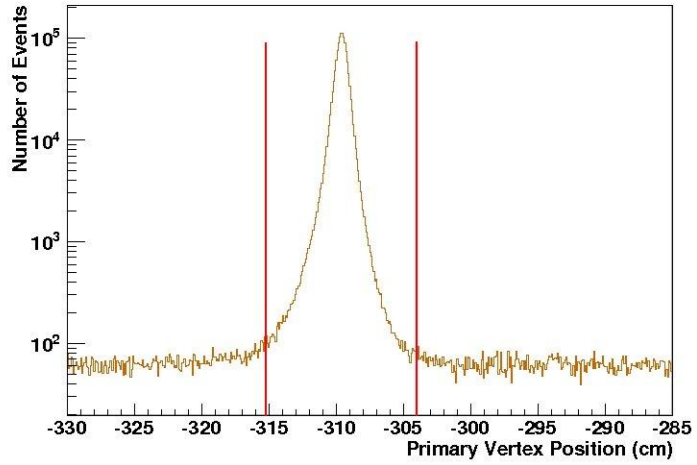

Figure 11: Primary vertex z position in the vicinity of the copper target (logarithmic scale). The red lines define the target region.

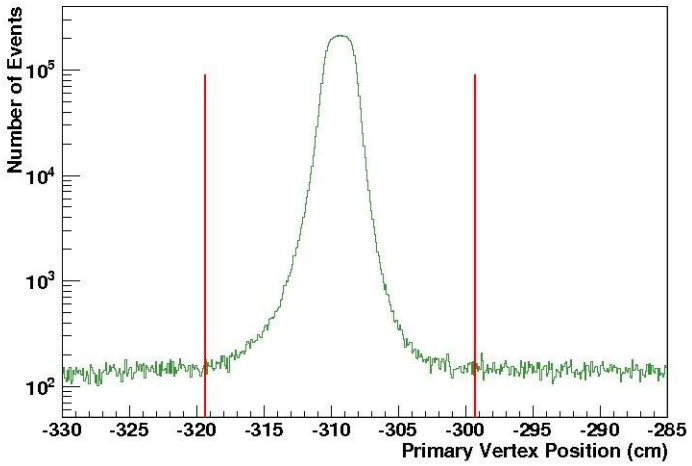

Figure 12: Primary vertex z position in the vicinity of the carbon target (logarithmic scale). The red lines define the target region.

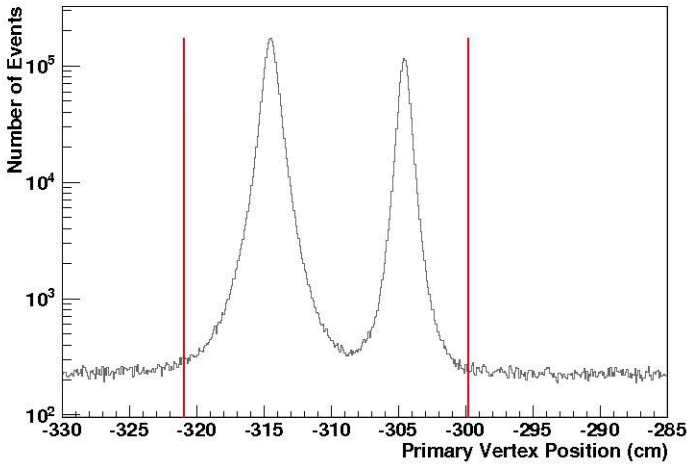

Figure 13: Primary vertex z position in the vicinity of the lead target (logarithmic scale). The red lines define the target region.

4.3 t-Distributions

One important kinematical variable to describe the diffractive dissociation of pions[9], is the square of the four momentum t transfered from the incoming pion to the outgoing system:

$$t = (p_a - p_c)^2 \tag{13}$$

where a and c are the indices that represent the incoming particle and the outgoing system, respectively.
In the analysis it is assumed that all the incoming particles are pions but as already mentioned before (see 1), there are some other particles in the beam (e.g. kaons) which can be used for luminosity normalization. Therefore, it is useful to introduce another kinematical variable which is independent of the mass of the incoming particle:

$$|t'| = |t| - |t|_{\min} \tag{14}$$

where $|t|_{\min}$ is the minimum value of $|t|$ required to produce a state with mass m_c. The variable $|t_{min}|$ has to be calculated for each event individually. An approximate calculation of $|t|_{min}$ in the laboratory system gives [Wei08]:

$$|t|_{\min} \approx \frac{(m_c^2 - m_a^2)^2}{4|\overrightarrow{p_a}|^2_{\text{lab}}} \tag{15}$$

In diffractive dissociation of hadrons, the radius of the diffracting object (the target nucleus) is given by [Aea76]:

$$R = 0.3\sqrt{|b|}\,\text{fm} \tag{16}$$

where b in $(\text{GeV}^2/c^2)^{-1}$ is the slope of the logarithm of the t distribution at low values of t. Therefore, as a cross-check, the t distributions have been plotted (in logarithmic scale) for different targets, and a line has been fitted to each histogram at linear part of the distribution at the low t region (Fig. 14, 15 and 16). The slopes for different targets are listed in table 4. Radii calculated by equation (16) are compared to the ones derived from the standard relation of the nucleus radius and mass number: $R \approx R_0 A^{1/3}, \quad (R_0 \approx 1\,\text{fm})$.

[9] A thorough explanation of diffractive dissociation of hadrons and its properties can be found in [Aea76].

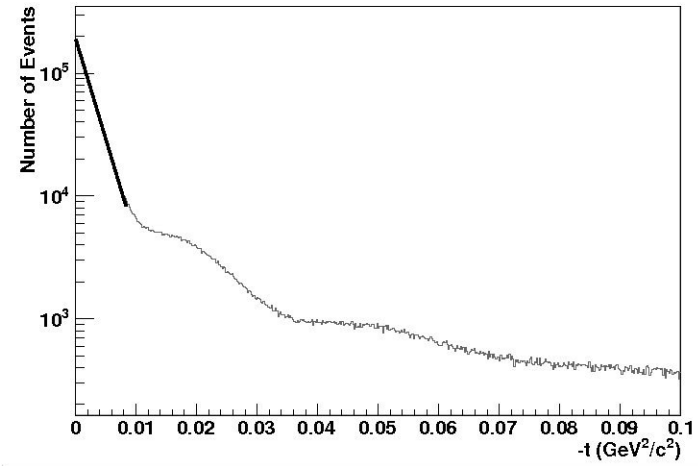

Figure 14: t-distribution at the target region for the exclusive events of the lead target (logarithmic scale). The black line represents an exponential fit at the low-t region.

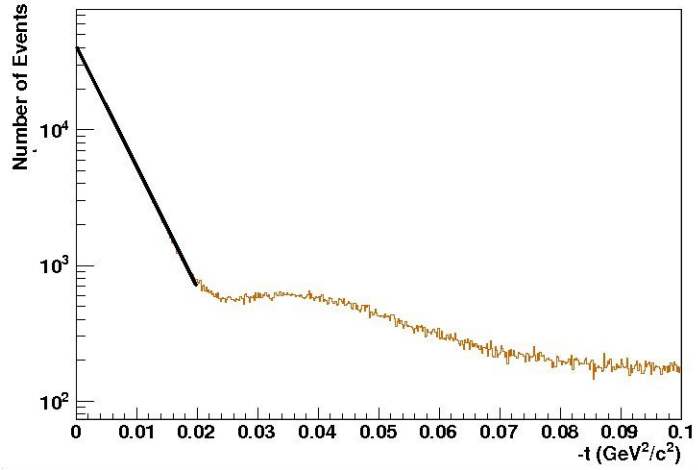

Figure 15: t-distribution at the target region for the exclusive events of the copper target (logarithmic scale). The black line represents an exponential fit at the low-t region.

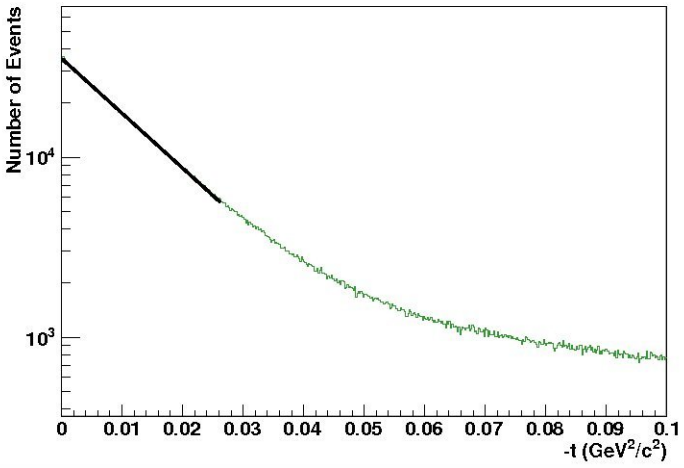

Figure 16: t-distribution at the target region for the exclusive events of the carbon target (logarithmic scale). The black line represents an exponential fit at the low-t region.

Target	**Pb**	**Cu**	**C**
Atomic mass (amu)	207.2	63.5	12
Slope (b)	-377.66 ± 0.33	-204.81 ± 0.24	-70.14 ± 0.1
R (calculated)	5.83 ± 0.01	4.29 ± 0.01	2.51 ± 0.01
R (theory)	5.8	4.2	2.6

Table 4: Comparison of radii of different nuclei derived from theory and the slope of the logarithm of the t distribution at low values of t.

5 Luminosity Normalization

In order to be able to compare any physical quantity for different targets which were used in the experiment, it is necessary to normalize the integrated luminosity associated with each target. In our study of color transparency, a relative normalization is sufficient and there is no need to estimate the absolute value of integrated luminosity.
There are different methods that can be applied. The most accurate method in our case, is counting the number of beam kaons which decay inside a certain z range during each time period. As a cross-check of this method a second method can be used, which is to estimate the overall beam flux during all analyzed runs. There are two ion chamber detectors responsible for flux measurement in COMPASS. Unfortunately, most of the values measured by these detectors during the two-week pilot run are not available anymore. Therefore, another method was introduced as a cross-check of the first method (counting the beam kaon decays), which is to estimate the sum of all spills [10] of the runs that each time period contains. This number correlates with integrated luminosity.

5.1 Counting the beam kaon decays

It is known that the hadron beam used in COMPASS in 2004, contains a certain amount of kaons ($K^-, \tau = 1.2 \cdot 10^{-8}$s) [Aea07]. These kaons may decay anywhere in the beam line. Assuming that all the decay particles are lost, there has been 3% kaon contamination in the π^- beam entering the experiment hall in COMPASS 2004 hadron program [COM]. It is possible to take advantage of beam kaon decays for normalizing the luminosity. In the early stages of this analysis (when the luminosity was being normalized) only events with 3 outgoing particles (2 of them with a negative electric charge and one with a positive electric charge) were subject of interest, therefore the hadronic decay $K^- \to \pi^-\pi^-\pi^+$ which has a branching ratio of 5.6% has been taken into account for this normalization. Later a broader range of interactions were let in but as it will be shown later, the luminosity normalization remains valid. Despite the small branching ratio, it is possible by applying some cuts to extract a clear K^- sample from all the events with $\pi^-\pi^-\pi^+$ in the final state. Therefore, assuming that there is a fixed ratio of kaons in the beam, and by comparing numbers of decays counted for runs dedicated to each target, a relative normalization of the beam intensity is feasible.

[10] One successful complete run contains 200 spills. During spills, beam particles are injected into the beam line. Each spill in 2004 was 4.8 s long within a 16.8 s long SPS cycle.

As already mentioned, to extract a clear sample of decaying kaons, it is necessary to introduce a number of cuts. These are: anti-target cut, momentum transfer cut and mass cut, and will be explained in the following sections.

5.1.1 Anti-target cut

Fig. 17 shows the primary vertex position along the z axis. The target sits at about $z = -310\,\text{cm}$. Further from the target there are much less interactions happening compared to the target region and therefore a cleaner sample of beam kaon decays is provided. At each side of the target there is a region with less interactions (no peak). The sources of these flat regions are the interactions considered as background. The same anti-target region is

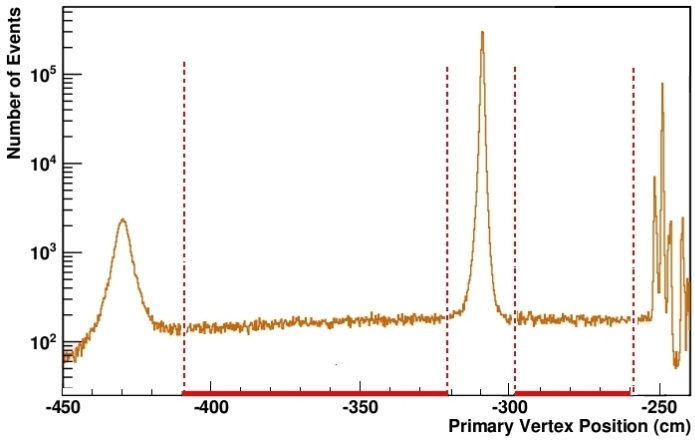

Figure 17: Primary vertex position along the beam axis for the copper target. The red area represents the anti-target regions.

defined for all targets, to avoid any inconsistency due to different acceptances in different z ranges. The anti target range is -410 – -321 cm upstream of the target and -299 – -259 cm downstream of the target. Knowing the opening of the SM1 magnet and its position on the z-axis the percent difference in acceptance at $z = -321\,\text{cm}$ and $z = -299\,\text{cm}$ can be estimated which is about 3%.

5.1.2 Momentum transfer cut

Theoretically, in a decay process theres is no momentum transfered to any nuclei, so in the analysis the momentum transfer of the events selected as kaon decays has to be assumed to be very close to zero. Only events with very

low momentum transfers ($< 10^{-3}\,\mathrm{GeV}^2/c^2$) have been taken into account (see Fig.18).

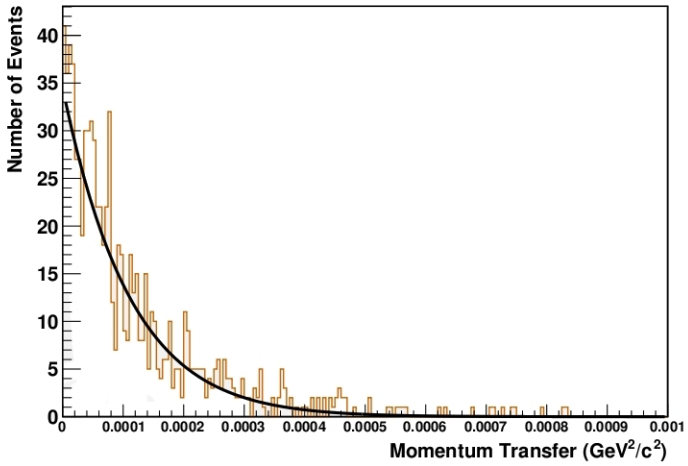

Figure 18: t'-distribution of the events selected for the luminosity normalization (Pb target).

5.1.3 Mass cut

To clear the data sample from interactions other than kaon decays a cut on the mass is also needed, so that only kaons enter the final data set. If the mass of the three outgoing particles ($\pi^-\pi^-\pi^+$) of the exclusive events at very low values of t is plotted, a sharp peak at about the nominal kaon mass ($494\,\mathrm{MeV}/c^2$) can be seen (Fig.19).

5.1.4 Summary

For each of the three target materials the primary vertex distribution was plotted by applying the cuts explained above in these ranges:

- Momentum transfer: $|t| < 0.001\ \mathrm{GeV}^2/c^2$.
- Anti-target cut: $-410 < z < -321\,\mathrm{cm}$ and $-299 < z < -259\,\mathrm{cm}$.
- Mass cut: $494 \pm 5\,\mathrm{MeV}/c^2$.
- Exclusivity cut on energy as explained in the previous chapter.

The number of interactions remaining after applying all these cuts, was considered as the number of beam kaon decays in the z regions mentioned above.

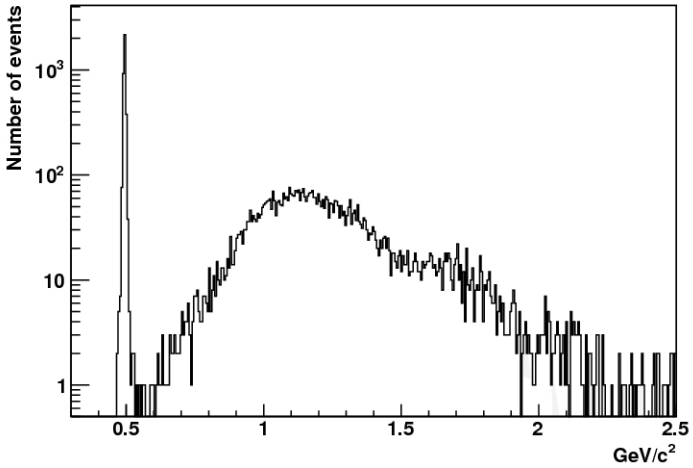

Figure 19: Invariant mass of the three outgoing particles ($\pi^-\pi^-\pi^+$) at very low values of t at the anti-target regions.

5.2 Sum of spills

The beam intensity at COMPASS is measured by two ion chamber detectors the muon chamber and the ion chamber placed at the beam line before it enters the COMPASS hall. Unfortunately most of the beam intensity values stored in the databases in 2004 are not available anymore.
Assuming that the beam intensity was not altered drastically during different runs then, counting the number of spills in each run and adding them up and comparing these numbers to the results of the previous method, will be a good way to make sure that there is no huge error in the luminosity normalization. A php script was written to sum up the number of spills of all the runs which were studied in this analysis, for each of the targets, using the COMPASS 2004 hadron run data which is stored in different MySQL databases.

5.3 Calculation of the normalization factors

The integrated beam luminosity can be expressed as:

$$L_{\text{int}} = \int L dt = N_B \cdot n_T \tag{17}$$

where n_T is the effective target thickness (the areal density) and N_B is the total number of particles of the incident beam [Sea08]. The areal density can be derived as:

$$n_T = \rho_T \cdot x_T \cdot \frac{N_A}{A} \tag{18}$$

Material	ρ (g/cm^3)	x_T (cm)
Pb	11.35	0.3
Cu	8.96	0.35
C	2.2	2.3

Table 5: Values used for the luminosity normalization

where ρ_T is the target density, x_T is the target thickness and A is surface area of the target which is the same for all targets (see section 3.4.2). The sum of spills (N_S) or sum of beam kaon decays (N_K) for each target in the corresponding running periods is proportional to the total number of particles of the incident beam. By calculating ($N_S \cdot n_T$) or ($N_K \cdot n_T$) for each target and finding the ratios of the results, it is possible to calculate the relative normalization factors.

$$M = x_T \cdot \rho_T \cdot N_K \text{ (or } N_S) \tag{19}$$

For the relative normalization, the normalization factor (F) of Pb is assumed to be one and the other factors are calculated relative to Pb, as follows:

$$F_{Pb} \equiv 1 = M_{Pb}/M_{Pb} \tag{20}$$
$$F_{Cu} = M_{Pb}/M_{Cu} \tag{21}$$
$$F_C = M_{Pb}/M_C \tag{22}$$

5.4 Results

5.4.1 Results from counting the kaon decays

In Fig. 20 (right) the mass distribution (around kaon mass) for the events selected as described in section 5.1 is plotted. The plot on the left side corresponds to the same events, only the events from the anti-target region upstream of the target are excluded. Gaussian functions have been fitted to both histograms and as it can be seen in the left plot (only the anti-target region downstream of the target included) the Gaussian fit has a smaller width corresponding to a better mass resolution. The worse mass resolution in the other plot is due to multiple scattering in the target region. Therefore, for having a cleaner sample of beam kaons, only events with a primary vertex position downstream of the target, are taken into account.

The number of beam kaon decays counted at the anti-target region downstream of the target, and the normalization factors which are calculated based on these numbers, are listed in table 6.

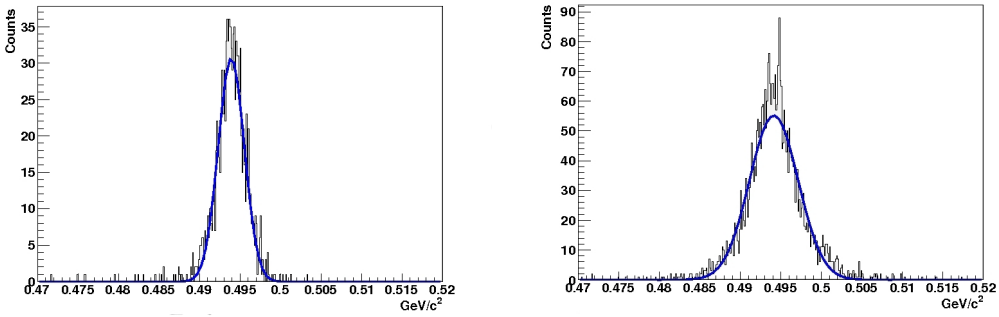

Figure 20: Kaon mass peak. Right: both anti-target regions included. Left: the anti-target region upstream of the target excluded.

Target	**Cu**	**C**	**Pb**
Number of decays	845	1059	2886
M	2687.78	5599.46	9826.83
F (relative to Pb)	3.66	1.75	1

Table 6: Values used for luminosity normalization based on counting the number of beam kaon decays.

5.4.2 Results from counting the number of spills

The luminosity normalization is done as in the previous method, only the number of beam kaon decays N_K is substituted by the number of spills N_S. The results are presented in table 7.

Target	**Cu**	**C**	**Pb**
Number of runs	20	22	58
Number of spills	2803	3545	8600
M	8915.78	18744.19	29283.00
F (relative to Pb)	3.28	1.56	1

Table 7: Values used for luminosity normalization based on counting the number spills.

5.4.3 Comparison of the results

The percent difference of the two sets of results is calculated as:

$$d = \frac{|F_1 - F_2|}{(F_1 + F_2)/2} \times 100 \tag{23}$$

where $F_1(F_2)$ denotes the normalization factor calculated based on the first (second) method. The percent differences are listed in table 8.

Target	F_1	F_2	d
C	1.75	1.56	5.7 %
Cu	3.66	3.28	5.5 %

Table 8: Percent differences of luminosity normalization factors.

The percent differences not being too high, proves that both methods of luminosity normalization are in good agreement and that the results of the more precise method (counting the number of kaon decays) can be trusted for the further steps of this analysis. The normalized t-distributions are shown in Figs. 21 and 22

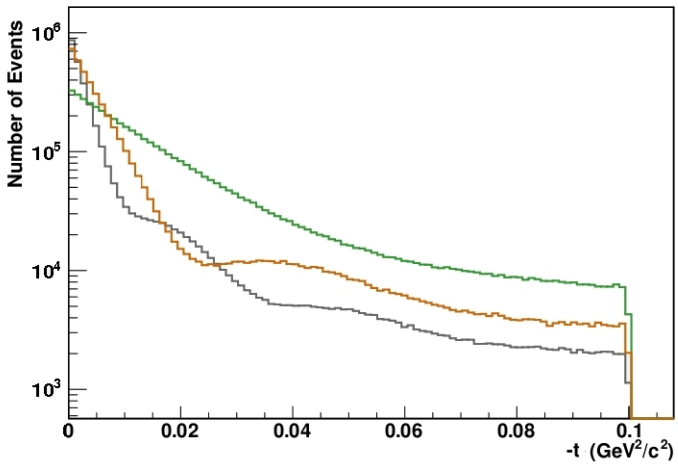

Figure 21: t-distribution of the three targets relatively normalized to luminosity (logarithmic scale). Grey curve: lead target, brown curve: copper target, green curve: carbon target.

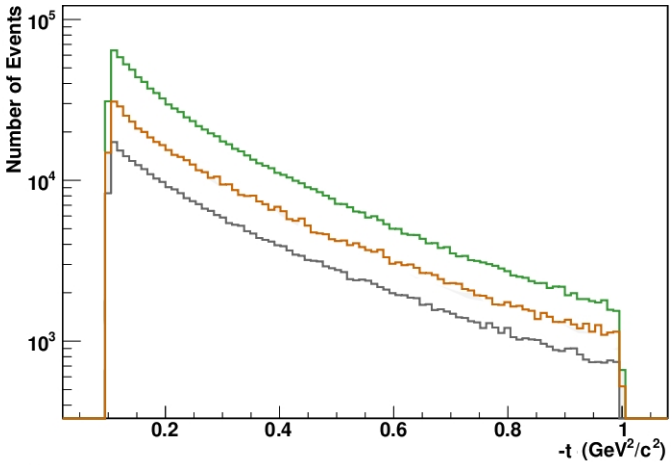

Figure 22: t-distribution of the three targets relatively normalized to luminosity (logarithmic scale). Grey curve: lead target, brown curve: copper target, green curve: carbon target.

6 Jet Finding

In hard scattering processes, jets are produced by hadronization of quarks and gluons. In this process, the colored partons are transformed into colorless hadrons. So, the observed jets provide a view of the underlying hard quark and gluon interactions that occur at very small distance scales. However, this view is inevitably clouded by the subsequent long distance hadronization of the primary quarks and gluons. For this reason, there can be no *unique* association of a jet of hadrons with a single initial quark or gluon [ES93]. Nevertheless, with a suitable jet-finding algorithm it is possible to minimize the effect of long distance physics and of the inherent jet ambiguities and obtain a fairly precise picture of the short distance dynamics. For selecting a data set containing jets, nearby hadrons which are traced by tracking detectors, can be chosen such that kinematic properties of the jets (e.g. momenta) can be related to the corresponding properties of the hadrons. The hadrons can be nearby in angle or in momentum space. The first leads to cone-based algorithms (used in hadron colliders) and the latter to the cluster-based algorithms (used in ee and ep colliders) [Zyc05].
For this analysis it is required to choose events where a pion diffractively dissociates to two mini-jets. Since COMPASS is a fixed target experiment and the energies involved (center-of-mass energy $\sqrt{s} \simeq 17$ GeV) are not as high as collider experiments – where large jets are produced – the term mini-jet is used. After the primary event selection, the outgoing hadrons are combined into groups of particles. Each of these groups is considered as a jet. Events with two jets are selected and further cuts (which are explained in the next chapter) are applied to choose the data sample suitable for this analysis.

6.1 Event Selection

Event selection is done via a UserEvent function as it was done for the luminosity normalization. The same quantities are checked and same cuts on energy and vertices and their positions are applied. Since a grouping is performed, events with any number of outgoing particles can be selected as long as all the other requirements are fulfilled. No matter how many outgoing particles one event contains, the sum of electric charges of these particles has to be equal to $-1\,\mathrm{e}$. This is because the beam particle is a π^- (same as the 3π events used for the luminosity normalization). Number of outgoing particles of the primary vertices are shown in Fig. 23.

Since the neutral particles cannot be reconstructed as precisely as the

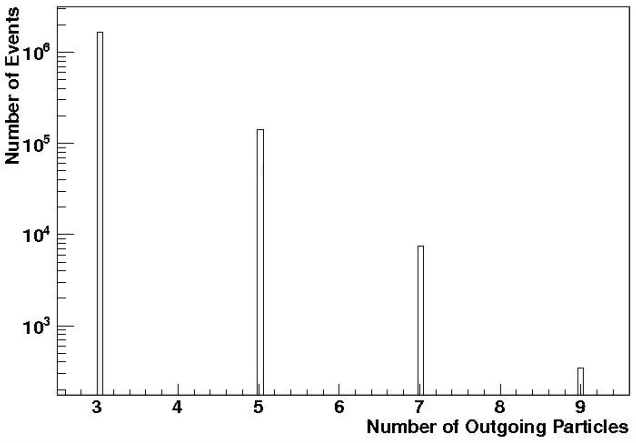

Figure 23: Number of outgoing particles of the primary vertices (Copper target, logarithmic scale).

charged particles, in order to minimize the ambiguities in the analysis, final states which contain π^0 particles are not taken into account. Therefore, the grouping of hadrons is done only when the number of outgoing particles is odd and obviously greater than 1.

6.2 Jet Finding Algorithm

Having a suitable algorithm for jet-finding was an important part of this study since it directly influences the results. The "JADE" cluster-based algorithm was chosen as a guideline for the algorithm used for this analysis. This algorithm was first used at the JADE detector at PETRA[11] [Bea86]. The same algorithm is used by the E791 collaboration at Fermilab for studying color transparency via diffractive dissociation of pions into two mini-jets (see Section 2.2.1). The key parameter of the JADE algorithm is a threshold mass, which has to be chosen before the grouping starts (this is explained in more detail in Section 6.2.1).
After selecting the threshold mass, the invariant masses of all possible pairs of outgoing particles are calculated

$$M_{lk} = (p_l + p_k)^2 \tag{24}$$

the indices l and k can represent any of the particles. Then the pair with the lowest invariant mass is identified. If the invariant mass of that

[11] **P**ositron-**E**lektron **T**andem **R**ing **A**nlage.

pair is lower than the threshold mass, the particles forming this pair are combined and considered as a pseudo-particle or a cluster. The pseudo-particle's four-momentum is equal to the sum of the four-momenta of the two particles/pseudo-particles forming it. After the first grouping, the process is repeated the same way with the new set of particles and pseudo-particles until no further clustering can be performed. If at any step the invariant mass of the pair with the lowest mass is higher than the threshold mass, the grouping is stopped. The number of clusters left at the end of the grouping process is called the jet- or the cluster-multiplicity of the event [Bea86].
The flowchart in Fig. 24 illustrates this algorithm. In Fig. 25 pairmasses at different steps of jet-finding process are plotted. The highest curve correspond to the pair masses before the grouping starts.

6.2.1 Determination of the threshold mass

Order of magnitude of the threshold mass can be determined by calculating the coherence length corresponding to our experiment. As explained in the second chapter the coherence length l_c should be long enough so that the PLC does not expand while traversing the nucleus. So it is required that $l_c \sim 10\,\mathrm{fm}$. The threshold mass should be of the same order of magnitude as the di-jet mass (M_J), which can be calculated using Eq. 2:

$$l_c = \frac{2p_{\mathrm{lab}}}{M_J^2 - m_\pi^2} \sim 10\,\mathrm{fm} \Rightarrow M_J \sim 5\,\mathrm{GeV}/c^2 \tag{25}$$

Therefore, the threshold mass is set to 3 GeV which is of the same order of magnitude as is above the mass of all known resonances. In Fig. 26 only events with three outgoing particles are plotted. The highest curve (dark green) represents the pair masses before any grouping is performed. The light green curve shows the pair masses at the same step but belongs only to those events that have been accepted as two-jet events at the end of jet-finding process. The blue curve corresponds to pair masses after the first step of grouping (in this case the only step). The red line shows the threshold mass. So all the events, to the right of the blue curve are accepted and the ones to its left are rejected.

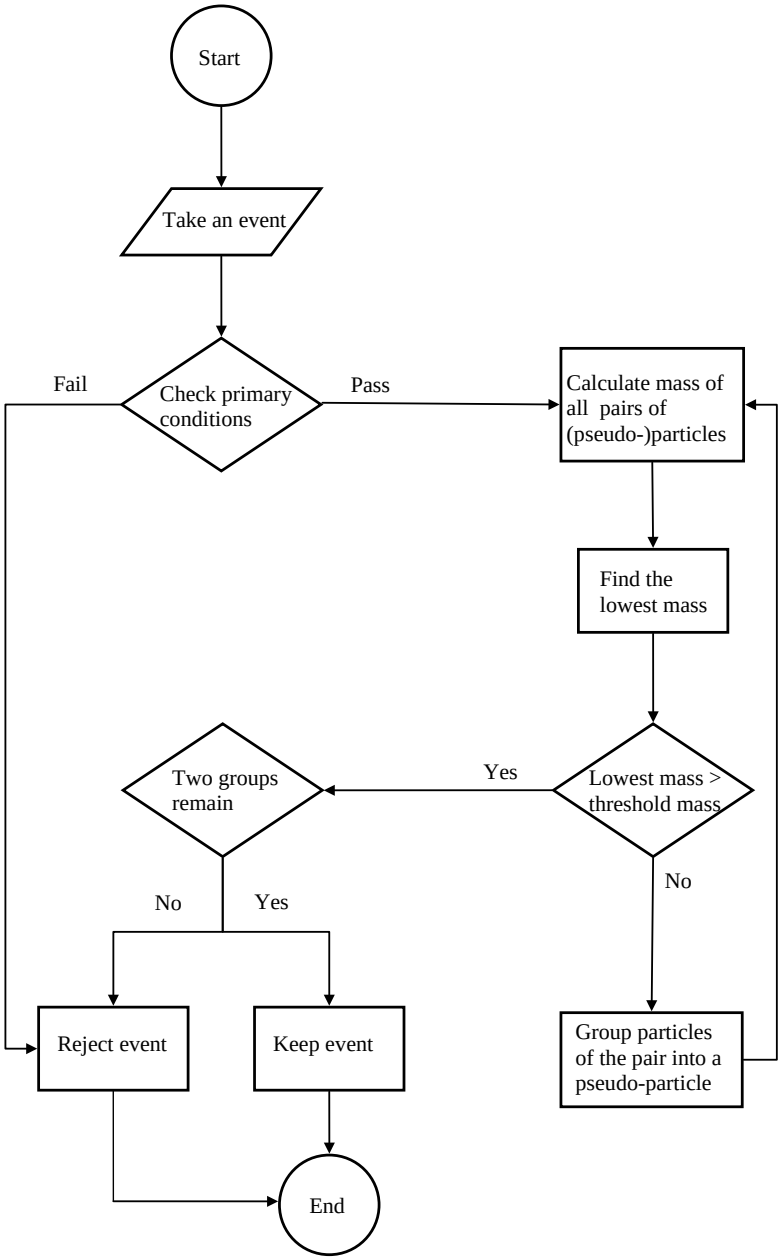

Figure 24: Mini jet finding algorithm.

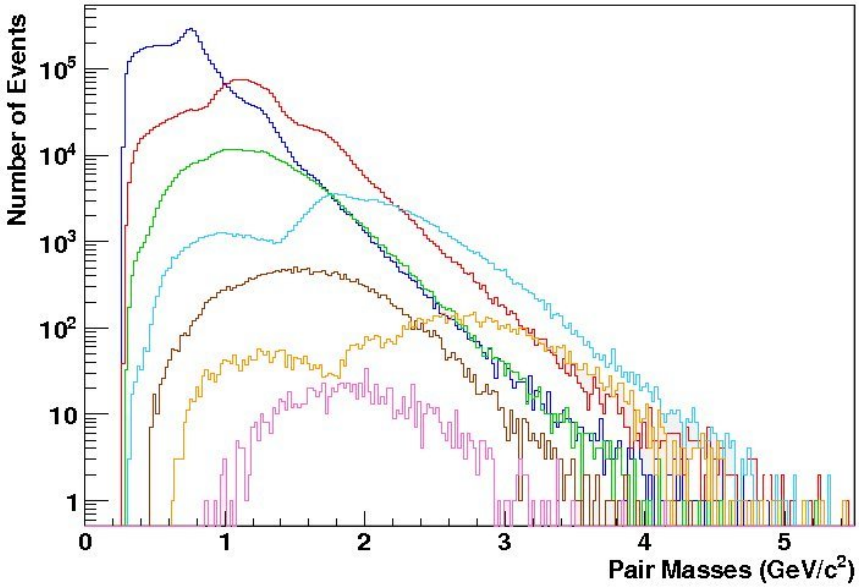

Figure 25: Pair masses at different steps of grouping with the jet-finding algorithm. The higher a curve is, to an earlier stage of the process it belongs (Copper target, logarithmic scale, threshold mass=3 GeV/c^2).

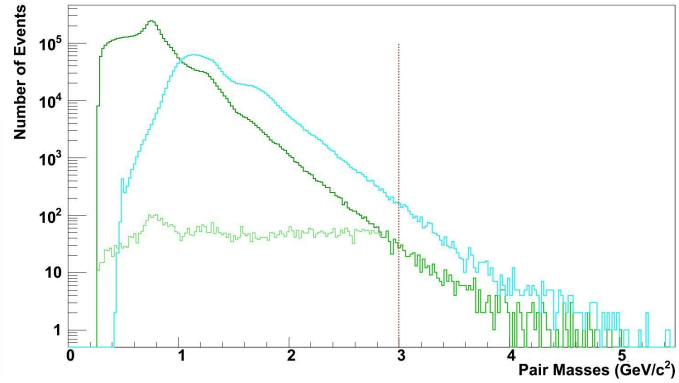

Figure 26: Pair masses at different steps of grouping with the jet-finding algorithm. The higher a curve is, to an the earlier stage of the process it belongs (Copper target, logarithmic scale).

7 Analysis

7.1 Relative mini-jet production cross-sections

Coherent diffractive dissociation of hadrons into high-p_T di-jets, provides a direct method to investigate color transparency effects. For CT the t-integrated cross-section of coherent diffractive production of high p_T di-jets, one expects that the cross-section for nuclear target is related to that for the nucleon target by [Sea01]

$$\frac{d\sigma}{st}(\pi A \to JJA)|_{t\approx 0} = A^2 \frac{d\sigma}{dt}(\pi N \to JJN)|_{t\approx 0} \tag{26}$$

Gluon shadowing/antishadowing in nuclei is neglected in this formula. For the t-integrated coherent cross-section, measured in experiments, CT predicts an approximate $A^{4/3}$ dependence (the exact value depends on the value of the transverse momentum of jets k_T). Otherwise, if the color-singlet objects, while propagating in nuclear matter, interact with nucleus with large cross-sections, the expected A-dependence is weaker. A ($\sigma \propto A^{2/3}$) dependence is typical for cross-sections comparable or larger than the cross-section of soft diffraction of pions by nuclei [Sea01, Fea02].
The cross-section per nucleus for the process can be parametrized as [Aea01]:

$$\sigma = \sigma_0 A^{\alpha} \tag{27}$$

Therefore, the relative mini-jet production cross-section can be written as:

$$\frac{\sigma_1}{\sigma_2} = (\frac{A_1}{A_2})^{\alpha} \tag{28}$$

indices 1 and 2 represent different types of target materials. α can be derived from the equation above,

$$\alpha = \frac{log(\sigma_1/\sigma_2)}{log(A1/A_2)} \tag{29}$$

7.1.1 Data sample

Selection of the data sample and jet-finding procedure are explained in chapters 4 and 6. Events with jet multiplicity equal to 2 are chosen for this analysis. Besides, a cut on momentum transfer is applied ($|t| < 0.01$) to ensure that the data sample mostly consists of coherent events. k_T distribution of the two jets (after applying all the cuts) is shown in Fig. 27.

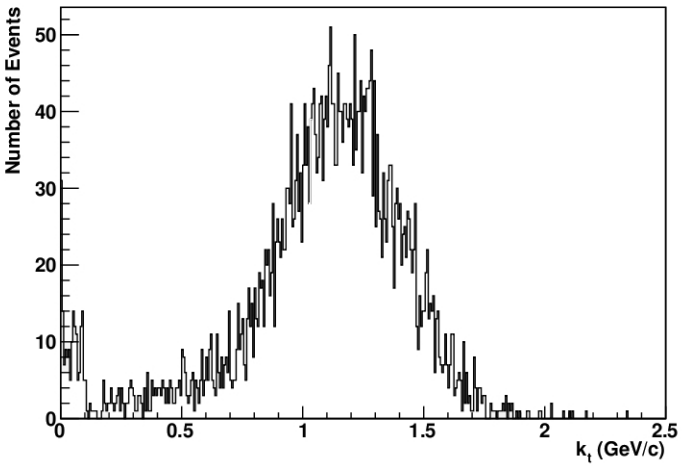

Figure 27: k_T-distribution of one the two jets (copper target).

7.2 Background extraction

In order to obtain a cleaner sample of di-jet events and to have a higher statistics, it is possible to extract the background interactions. For this purpose, Monte Carlo simulations are suitable. Because of time limits this could not be achieved for this analysis but can be done later for improving the results.
The method used in this study is backward extrapolation. A line is fitted to the t-distribution where $-t \sim 0.1 - 0.3\,\mathrm{Gev}^2/c^2$. In this region, most of the events are incoherent interactions. By extrapolating this line back to the lower values of t, contributions of incoherent interactions can be subtracted from the data set. After subtracting the background the t region included in the analysis is extended up to $-t < 0.1\,\mathrm{GeV}^2/c^2$.

7.3 Results from previous experiments and theoretical predictions

Results from the similar study at the E791 at Fermilab and theoretical predictions of color transparency are listed in table 9.

k_T bin (GeV/c)	α	$\Delta\alpha_{\text{stat}}$	$\Delta\alpha_{\text{sys}}$	$\Delta\alpha$	α(CT)
1.25 - 1.5	1.64	$\pm$0.05	+0.04 -0.11	+0.06 -0.12	1.25
1.5 - 2	1.52	$\pm$0.09	$\pm$0.08	$\pm$ 0.12	1.45
2.0 - 2.5	1.55	$\pm$0.11	$\pm$0.12	$\pm$0.16	1.60

Table 9: α based on the color-transparency predictions and experimental results for coherent dissociation of pions from the E791 experiment [Ait01].

7.4 Results

For calculating α, normalized number of coherent events (N) is estimated and the σ_1/σ_2 in eq. 29 is substituted by N_1/N_2. The normalization is done based on the values calculated in chapter 5. Three k_T bins have been used: 1 - 1.25 GeV/c, 1.25 - 1.5 GeV/c, 1.5 - 2 GeV/c. The results are shown in tables 10, 11 and 12. These results are obtained before background extraction. For three types of target materials two independent values for α can be estimated.

Targets	$\log(A_1/A_2)$	$\log(N_1/N_2)$	α	$\Delta\alpha_{\text{stat}}$
Cu/Pb	-0.51	0.09	-0.17	0.1
C/Pb	-1.24	-0.17	0.14	0.04

Table 10: Estimated values of α without background extraction, k_T-bin: 1 - 1.25 GeV/c.

Targets	$\log(A_1/A_2)$	$\log(N_1/N_2)$	α	$\Delta\alpha_{\text{stat}}$
Cu/Pb	-0.51	0.07	-0.14	0.11
C/Pb	-1.24	-0.23	0.19	0.04

Table 11: Estimated values of α without background extraction, k_T-bin: 1.25 - 1.5 GeV/c.

For extracting the background events with $1 < k_T < 2$ are all analyzed together. If events are analyzed in different k_T bins, there will not be enough statistics at high t region and making an acceptable fit to the t distribution at high values of t would be impossible. Results after background subtraction are summarized in table 13.

Targets	$\log(A_1/A_2)$	$\log(N_1/N_2)$	α	$\Delta\alpha_{\text{stat}}$
Cu/Pb	-0.51	0.05	-0.10	0.16
C/Pb	-1.24	0.7	-0.56	0.07

Table 12: Estimated values of α without background extraction, k_T-bin: 1.5 - 2 GeV/c.

Targets	$\log(A_1/A_2)$	$\log(N_1/N_2)$	α	$\Delta\alpha_{\text{stat}}$
Cu/Pb	-0.51	0.69	-1.36	0.94
C/Pb	-1.24	0.34	-0.27	0.39

Table 13: Estimated values of α after subtracting the background, $1 < k_T < 2$ GeV/c.

8 Summary and Outlook

Color transparency is a phenomenon predicted by perturbative QCD which predicts that small singlet systems of quarks and gluons interact with hadrons with small cross-sections. The color transparency phenomenon can be observed in diffractive dissociation of pions into di-jets. Pions that scatter coherently from different target materials into di-jets can be studied for this purpose. The per-nucleus cross-section of this process is parametrized as $\sigma = \sigma_0 A^\alpha$. Theoretical calculations of color-transparency, predict values near 1.6 for α. The exact value of α depends on jet transverse momentum. This process is studied in this thesis
This work is based on the data taken at a two-week pilot run in 2004 at the COMPASS experiment at CERN. It makes use of a 190 GeV/c pion beam and three different types of target materials (carbon, copper and lead). Luminosity is normalized and relative mini-jet production cross-sections are calculated and are shown in chapter 7 (numbers obtained in this chapter are normalized to luminosity). Our results are not consistent with theoretical predictions. This can be due to several reasons which can be investigated in detail in a future study. Some of the most important aspects are listed bellow:

1. The background interactions can be extracted in a more precise way using Monte Carlo simulations.

2. The systematic errors can be estimated and taken into account.

3. The threshold mass used in the jet-finding algorithm can be optimized for this study by using Monte Carlo simulations.

Suggestions for further studies: By improving the di-jet selection, the data sample can be used for a direct measurement of the pion valence quark momentum distribution. Diffractive dissociation of a pion into jets is a coherent process in which the quark and anti-quark in the pion hadronize into two jets. Assuming that in this fragmentation process each quark's momentum is transfered to a jet, measurement of the jet momenta gives the quark and anti-quark momenta [Ait08]:

$$x_{\text{measured}} = \frac{p_{\text{jet1}}}{p_{\text{jet1}} + p_{\text{jet2}}} \tag{30}$$

If the momentum distribution of valence quarks are studied, the results can be compared to functions which are calculated by using perturbative methods

that describe the momentum distribution amplitude for the quark and anti-quark in the $|q\overline{q}\rangle$ configuration. More information on these functions and results from the E791 experiment at Fermilab can be found in [Aea08].

List of Figures

List of Tables

References

[Aea76] U. Amaldi et al. Diffraction of hadronic waves. *Ann. Rev. Nucl. Sci.*, 26:385–456, 1976.

[Aea01] E.M. Aitala et al. Observation of color-transparency in diffractive dissociation of pions. *Phys.Rev.Lett.*, 86:4773–4777, 2001.

[Aea07] P. Abbon et al. The compass experiment at cern. *Nuclear Instruments and Methods in Physics Research Section A*, 577(3):455–518, 2007.

[Aea08] E.M. Aitala et al. Direct measurement of the pion valence-quark momentum distribution, the pion light-cone wave function squared. *Physical review letters*, 86:4768–4772, 2008.

[Bea83] G. Bertsch et al. Diffractive excitation in quantum chromo dynamics. *Physical review letters*, 47(5):297–300, 1983.

[Bea86] W. Bartel et al. Experimental studies on multijet production in positron-electron annihilation at petra energies. *Zeitschrift fuer Physik C*, 33:4768–4772, 1986.

[Bea93] B. Blaettel et al. How transparent are hadrons to pions? *Physical Review Letters*, 70(7):896–899, 1993.

[Cea08] S. U. Chung et al. Diffractive dissociation for compass. unpublished COMPASS note, April 2008.

[COM] COMPASS web site. wwwcompass.cern.ch.

[ES93] S.D. Ellis and D.E. Soper. Successive combination jet algorithm for hadron collisions. *Physical Review D*, 48:3160–3166, 1993.

[Fea93a] L. Frankfurt et al. Coherent nuclear diffractive production of minijets- illuminating color transparency. *Physics Letters B*, 304(1,2):1–7, 1993.

[Fea93b] L. Frankfurt et al. Evidence color fluctuations in hadrons from coherent nuclear diffraction. *Physical Review Letters*, 71(18):2859–2862, 1993.

[Fea01] L. Frankfurt et al. Color coherent phenomena on nuclei and the qcd evolution equation. *Journal of Physics G: Nuclear and Particle Physics*, 27:R23–R68, 2001.

[Fea02] L. Frankfurt et al. Coherent qcd phenomena in the coherent pion-nuclear and pion-nuclear production of the two jets at high relative momenta. *Physical Review D*, 65:1–26, 2002.

[Gra05] S. Grabmueller. Studies of diffractive particle production at compass. Master's thesis, Technische Universität München, December 2005.

[Hea06] K. Hafidi et al. Study of color transparency in exclusive vector meson electroproduction off nuclei. July 2006.

[Lev08] S. Levorato. *Measurement of Transverse Spin Effects in COMPASS on Polarized Proton Target*. PhD thesis, Università Degli studi di Trieste, 2008.

[Pre07] J. Pretz. The gluon polarization in the nucleon from the compass experiment. Habilitation's thesis, Rheinischen Friedrich-Wilhelms-Universitaet Bonn, April 2007.

[ROO] ROOT web site. http://root.cern.ch.

[Sea01] A. Sandacz et al. Color transparency at compass. COMPASS note 2001-4, March 2001.

[Sea08] H.J. Stein et al. Determination of target thickness and luminosity from beam energy losses. *Physical Review Special Topics - Accelerators and Beams*, 11(5):1–11, 2008.

[Web04] R. Webb. *First Measurements of Transverse Spin Asymmetries through Single Pion Production at the COMPASS Experiment*. PhD thesis, Fredrich-Alexander-Universität Erlangen-Nuremberg, 2004.

[Wei08] Q. Weitzel. *Precision Meson Spectroscopy: Diffractive Production at COMPASS and Development of a GEM-based TPC for PANDA*. PhD thesis, Technische Universität München, September 2008.

[Zyc05] P. Zych. Diffractive dissociation for compass. Presentation at CMS Warsaw Physics Gathering, May 2005.

Acknowledgement

In the first place, I thank most sincerely Prof. Dr. Stephan Paul for giving me the opportunity of working at the E18. Without his support and encouragement, this work would not be possible. I appreciate his experience and knowledge in the field of particle physics which added considerably to my graduate skills.
I would like to thank Dr. Bernhard Ketzer for his patience and support towards my thesis and all other academic activities. I appreciate his in-depth knowledge and his way of tackling physics problems.
Also, enormous thanks to Thiemo Nagel for the assistance and kindness he has provided throughout this project. His knowledge has allowed me to save a considerable amount of time.
My grateful thanks to all E18 members who succeeded in helping me at any moment.
Special thanks to Alexander Mann, Florian Schneider and Stefanie Grabmüller. We shared an office during the last year. They have always helped me whenever I needed help and we had a lot of fun together.
Majid, Mahsa, Sheema and Elham, I would like to thank you millions of times for your support. You have done a lot to help me with my thesis.
To my mother, father and brother I owe the deepest debt of gratitude. Without their profound love and support, it would not have been possible for me to achieve one of my most important goals, to erase some of the question marks I had in mind since my childhood and to implant many more instead.